

# Why calcium inhibits magnesium-dependent enzyme phosphoserine phosphatase? A theoretical study

Ling Yang · Rong-Zhen Liao · Wan-Jian Ding ·  
Kai Liu · Jian-Guo Yu · Ruo-Zhuang Liu

Received: 14 March 2012 / Accepted: 2 September 2012 / Published online: 13 September 2012  
© Springer-Verlag 2012

**Abstract** Phosphoserine phosphatase (PSP) utilizes one  $Mg^{2+}$  ion to catalyze the hydrolysis of phospho-L-serine. The displacement of  $Mg^{2+}$  by  $Ca^{2+}$  results in the loss of activity. The reaction mechanisms for the enzyme with both  $Mg^{2+}$  and  $Ca^{2+}$  bound were investigated using hybrid density functional theory. A large quantum chemical model abstracted from the X-ray crystal structure was employed in the calculations. Our calculations shed new insight into the catalytic mechanism of the natural enzyme and its lack of activity by  $Ca^{2+}$  substitution. For the catalytic reaction, our calculations showed that the whole reaction proceeds through two steps, namely dephosphorylation and phosphate hydrolysis. The associated barriers for these two steps are calculated to be 11.9 and 12.0 kcal mol<sup>-1</sup>, respectively. The Mg-bound Asp11 residue functions as a nucleophile to attack the phosphorus moiety, in

concomitant with the departure of the leaving group, which takes a proton from the neutral Asp13 residue. In the subsequent step, the newly formed anionic Asp13 residue activates a water molecule to perform the reverse attack on the phosphoryl intermediate, affording the phosphate product. The substitution of  $Mg^{2+}$  by  $Ca^{2+}$  results in different metal coordination fashion, in which the Asp167 residue changes from bidentate to monodentate and a second water molecule becomes ligated to  $Ca^{2+}$ . The calculated barriers for the hydrolysis are ca 8 kcal mol<sup>-1</sup> higher than those in the native enzyme, which reconciles with the fact that  $Ca^{2+}$  inhibits the activity of PSP. Several possible reasons are discussed.

**Keywords** Phosphoserine phosphatase · Magnesium · Calcium · Density functional calculations · Inhibition mechanism

**Electronic supplementary material** The online version of this article (doi:10.1007/s00214-012-1275-y) contains supplementary material, which is available to authorized users.

L. Yang  
Institute of Theoretical and Simulation Chemistry, Academy of Fundamental and Interdisciplinary Science, Harbin Institute of Technology, Harbin 150080, People's Republic of China

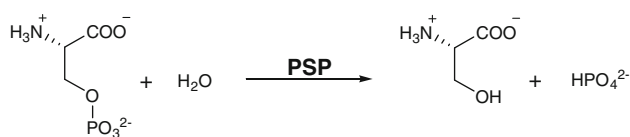
L. Yang · W.-J. Ding · J.-G. Yu (✉) · R.-Z. Liu  
College of Chemistry, Beijing Normal University,  
Beijing 100875, People's Republic of China  
e-mail: jianguo\_yu@bnu.edu.cn

R.-Z. Liao (✉)  
Max-Planck-Institut für Kohlenforschung, Kaiser-Wilhelm-Platz 1,  
45470 Mülheim an der Ruhr, Germany  
e-mail: rongzhen@kofo.mpg.de

K. Liu  
College of Life Science, Beijing Normal University,  
Beijing 100875, People's Republic of China

## 1 Introduction

Phosphoserine phosphatase (PSP, EC 3.1.3.3) is a mononuclear magnesium-dependent enzyme that catalyzes the hydrolysis of phospho-L-serine (PLS), leading to the formation of L-serine and inorganic phosphate (Pi) (Scheme 1) [1]. The product, L-serine, is not only the direct precursor of D-serine and a precursor for the biosynthesis of glycine but also an uncompetitive inhibitor of PSP [2–12]. PSP is a likely regulator of the steady-state D-serine level in brain, which is a crucial co-agonist of the N-methyl-D-aspartate (NMDA) type of glutamate receptors in mammalian tissues, especially in the nervous system [3–10]. It is possible to regulate NMDA activity by using selective inhibitors against serine racemase and/or PSP [2–12]. Thus, PSP may be an attractive target for inhibitor and drug design.



**Scheme 1** Reaction catalyzed by phosphoserine phosphatase

Amino acid sequence analysis has demonstrated that *Methanococcus jannaschii* PSP (MJPSP), the subject for this study, is a member of the haloacid dehalogenase (HAD) superfamily. The members in this family are characterized by three highly conserved sequence motifs: DXDX [T/V] [L/V], [S/T]XX, and K-[G/S][D/S]XXX[D/N] [3–10, 13]. The first aspartate residue in motif I functions as a nucleophile to start the reaction [3, 13, 14]. Mutation of the conserved residues shows that all three motifs play an important role in the catalysis [13–16]. MJPSP [1, 3, 17] and several other members of this family, such as human PSP (HPSP) [2, 18, 19], deoxynucleotidases (dNs) [20], haloacid dehalogenase [21], Ca-ATPase P-subunit [22], and  $\beta$ -phosphoglucomutase ( $\beta$ -PGM) [23], have similar  $\alpha/\beta$  fold and architecture of the active site but are able to catalyze different type of reactions. Wang et al suggested that the PSPs form a phospho-enzyme intermediate during the reaction [1, 3, 17], which is similar to the case of soluble nucleotidase presented by Allegrini [24].

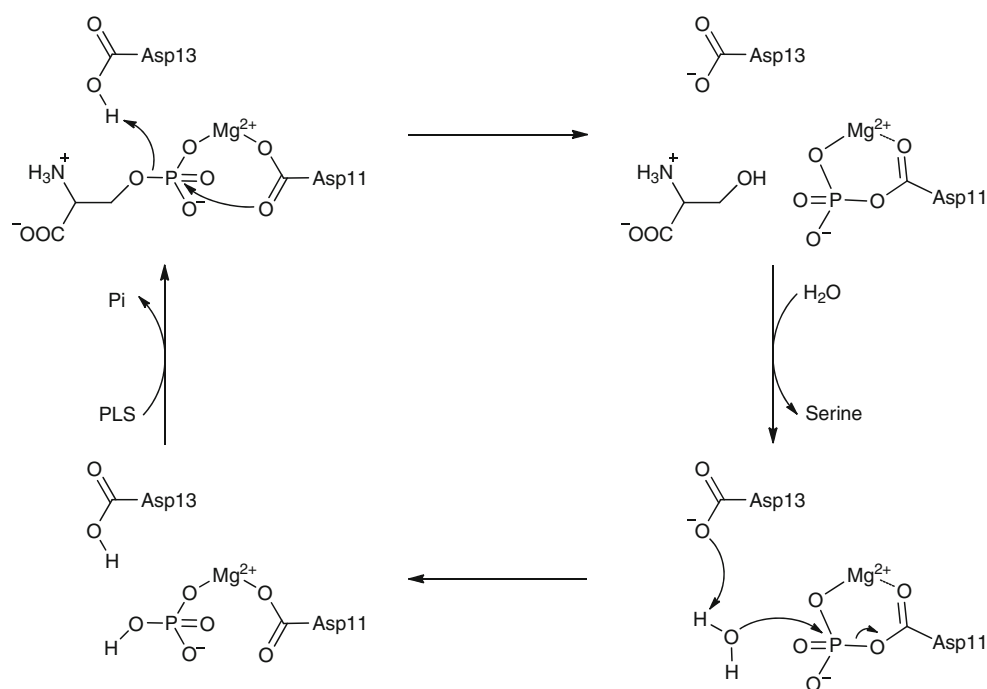
The X-ray crystal structure of MJPSP has been solved in complex with different inhibitors and transition state analogues [1, 3, 17]. The structure of MJPSP complexed with phosphate reveals a mononuclear magnesium center in the active site [3–10]. The first-shell coordination sphere includes the phosphate, two aspartates (Asp11, Asp167), the carbonyl group of the Asp13 backbone, and two  $\text{H}_2\text{O}$  molecules. Asp11 was suggested to perform the nucleophilic attack and get phosphorylated [3, 13, 14]. A second-shell residue, Asp13, which is believed to be the general acid to protonate the leaving group [13], forms two hydrogen bonds to Thr21 and the peptide backbone of Glu20-Thr21. In addition, a lysine (Lys144) and an arginine (Arg56) provide electrostatic interaction with the phosphate [1]. Furthermore, Asn170 and Ser99-Gly100 peptide backbone donate hydrogen bonds to the phosphate [1]. Kinetic studies of mutant enzymes showed that the mutation of the amino acid residues (D11E/N, D13E/N, S99A, K144A/R, and D167N) in the active site led to impaired catalytic activity, decreased substrate, or magnesium binding affinity [13–16]. Structure and mutagenesis studies indicate a critical role of Asp13 as a general acid/base in the phosphoryl transfer reaction [3–14].

The reaction mechanism of PSP has been put forward on the basis of structural [1, 3, 11, 19] and kinetic [13, 15, 16] studies, as well as theoretical calculations [25, 26]. Wang and coworkers suggested that the hydrolysis of PLS

proceeds through a stepwise phosphotransfer mechanism: the phosphoryl group is transferred from PLS to Asp11 via a penta-coordinated phosphorus intermediate, producing a labile phosphoenzyme intermediate and a serine molecule. In the following step, the phosphorylated PSP is hydrolyzed, releasing inorganic phosphate [1, 3]. In this mechanism, the retention of the phosphorus configuration is suggested. Due to the lability of the aspartyl-phosphate formed during the reaction, it is difficult to characterize such intermediate using experimental tools. In the crystal of MJPSP in complex with  $\text{BeF}_3^-$ , an aspartyl- $\text{BeF}_3$  structure is observed, which suggests an associative character during the phosphoryl transfer [17]. Based on QM/MM calculations, Re et al. suggested that the reversible phosphorylation of PSP proceeds with a concerted and geometrically associative (compact phosphorane-like) but electronically dissociative (metaphosphate-like) transition state, coupled with a proton transfer from Asp13 to the leaving group (Scheme 2) [25, 26]. However, for the hydrolysis reaction, their calculations showed that the reaction barrier of the backward reaction ( $2.7 \text{ kcal mol}^{-1}$ ) is much lower than that of the forward reaction ( $24.4 \text{ kcal mol}^{-1}$ ) [26]. This indicates that the hydrolysis cannot take place due to the higher barrier and also the large endothermicity (ca  $+22 \text{ kcal mol}^{-1}$ ), which thus cannot explain the catalysis for this enzyme.

Of particular interesting is that the incorporation of  $\text{Ca}^{2+}$  into the active site of PSP leads to the loss of the activity [2, 18, 19]. The inhibitory effect of  $\text{Ca}^{2+}$  on the  $\text{Mg}^{2+}$ -dependent PSP has been proposed to correlate with the difference in the coordination structures of  $\text{Ca}^{2+}$  and  $\text{Mg}^{2+}$  in the active site. Peeraer et al suggested that  $\text{Ca}^{2+}$  cannot provide the same metal-ligand binding pattern as  $\text{Mg}^{2+}$  and Asp11 may become bidentate to calcium [18, 19]. On the basis of the crystal structure of HPSP, Dudev and Lim proposed that a switch of the carboxylate-binding mode of Asp20 in HPSP (corresponding to Asp11 in MJPSP) from monodentate to bidentate takes place upon  $\text{Ca}^{2+}$  substitution, which abolishes the enzymatic activity [27]. Similar proposal has been put forward for  $\text{Mg}^{2+}$ -dependent *E. coli* ribonuclease H1 to explain the lack of activity by  $\text{Ca}^{2+}$  substitution [28]. DFT calculations by Dudev and Lim suggested that the favorable carboxylate-water hydrogen-bonding interaction in Mg complexes makes the monodentate carboxylate-binding mode preferred in magnesium proteins [29]. In spite of these possible explanations, exactly how calcium inhibits the activity of PSP is still not clear.

In the present work, density functional calculations were employed to investigate the inhibition mechanism of MJPSP by  $\text{Ca}^{2+}$  ion. A model of the active site was designed on the basis of the crystal structures (PDB ID: 1F5S), and potential energy profiles were calculated for

**Scheme 2** Suggested reaction mechanism for PSP [25, 26]

enzyme with both  $\text{Mg}^{2+}$  and  $\text{Ca}^{2+}$  ions as the cofactors employing the hybrid density functional method B3LYP [30–32]. This approach has previously been successfully applied to the study of a number of enzyme reaction mechanisms [33–54]. Including two recent studies on the reaction mechanisms of the related magnesium-dependent enzymes Deoxynucleotidases (dNs) [33], *Escherichia coli* inorganic pyrophosphatase (E-PPase) [44].

## 2 Computational details

The calculations presented herein were performed using the density functional method B3LYP [30–32] as implemented in the Gaussian03 program package [55]. Geometry optimizations were carried out with the 6-31G(d,p) basis sets for C, N, O, and H elements and the 6-311+G(d) for Mg, Ca, and P. On the basis of the optimized geometries, more accurate energies were obtained by performing single-point calculations with the 6-311++G(2d,2p) basis sets for all elements. For the phosphoryl transfer step with  $\text{Mg}^{2+}/\text{Ca}^{2+}$  ion, single-point calculations at the MPWB1K/6-311++G(2d,2p) [56] and BB1K/6-311++G(2d,2p) [57] levels based on the same optimized geometries were also carried out to evaluate the sensitivity of the energetics to the choice of different functionals. The calculated barrier of 13.8/19.8 and 13.7/19.8 kcal mol<sup>-1</sup> is very close to the barrier with B3LYP (11.9/18.4 kcal mol<sup>-1</sup>), further confirming the adequacy of B3LYP for this kind of applications.

The polarization effects of the enzyme environment were evaluated by performing single-point calculations on

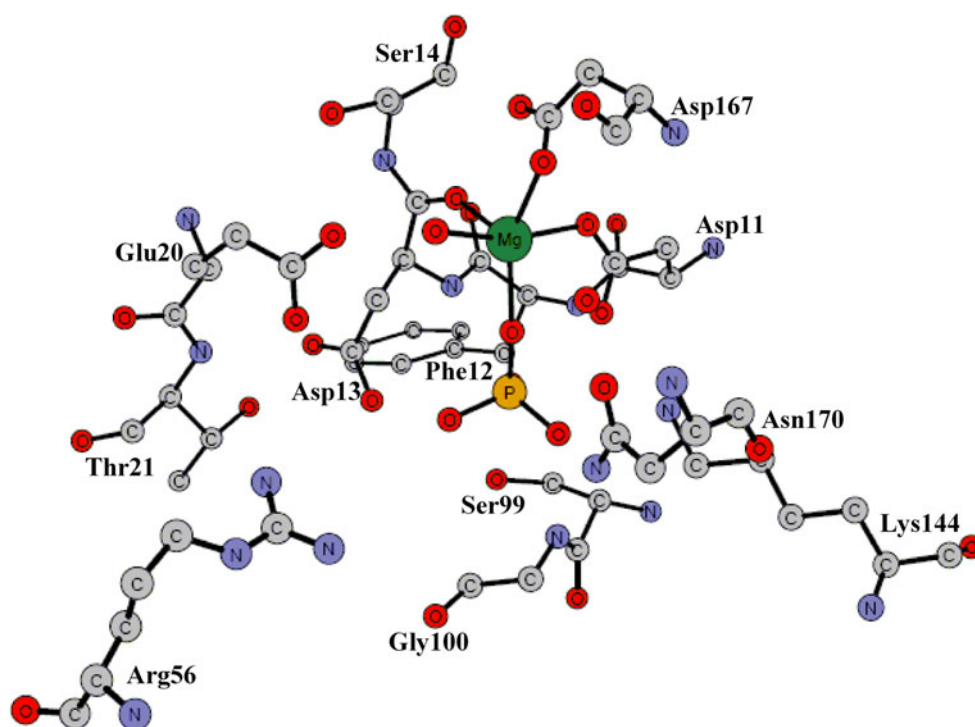
the optimized structures at the same theory level as the geometry optimizations using the conductor-like polarizable continuum model (CPCM) method [58–61]. The dielectric constant  $\epsilon$  was set to four, which is a value usually used in modeling protein surroundings.

Frequency calculations were performed at the same theory level as the geometry optimizations to obtain zero-point energies (ZPE) and to confirm the nature of various stationary points. As will be discussed below, some atoms were kept fixed to their X-ray crystal positions during geometry optimizations. This procedure leads to a few small imaginary frequencies, in this case on the order of  $10i$ – $40i$  cm<sup>-1</sup>. As they do not contribute significantly to the ZPE and can thus be ignored. However, they make the calculations of the harmonic entropy effects inaccurate. Therefore, entropy was not considered in the current study. In any case, entropy effects are expected to be rather small and do not alter any mechanistic conclusion, as shown, for example, by QM/MM-free energy calculations on histone lysine methyltransferase [62], *p*-hydroxybenzoate hydroxylase [63], 5'-fluoro-5'-deoxyadenosine synthase, P450cam, and chorismate mutase [64]. The energies reported herein are corrected with both solvation and zero-point energies.

## 3 Model of active site

Based on the crystal structure of MJPS (PDB ID: 1F5S) [3] (see Fig. 1), a model of the active site is devised. The model consists of the divalent metal center ( $\text{Mg}^{2+}$  in model A and  $\text{Ca}^{2+}$  in model B) and its first-shell ligands:

**Fig. 1** X-ray crystal structure of the active site of MJPSP in complex with a phosphate group bound (coordinates taken from PDB ID: 1F5S) [3]



carboxylate moieties of Asp167 and Asp11, backbone carbonyl group of Asp13, and two water molecules (Fig. 2). Asp13 is set to be neutral as the crystal structure of PSP suggests that it is in a protonated state [3] and its pKa value was 5.45 predicted by Re et al. [26] using PROPKA, which is shifted toward a basic region compared to the model value of Asp (3.80). Thus, it is believed to be the general acid to protonate the leaving group [3, 14]. Truncated models of the second-shell residues, Phe12, Ser14, Glu20-Thr21, Arg56, Ser99-Gly100, Lys144, and Asn170, are also included, as shown in Fig. 2. Hydrogen atoms are added manually. To keep the optimized structures close to the experimental one, some truncated atoms are kept fixed at their corresponding X-ray positions during the geometry optimizations. These atoms are labeled with asterisks in the figures below. The natural phospho-L-serine substrate was used to study the mechanism. The resulting model consists of 141 and 144 atoms for the dephosphorylation and phosphate hydrolysis reaction, respectively, and the total charge of the model is  $-1$ .

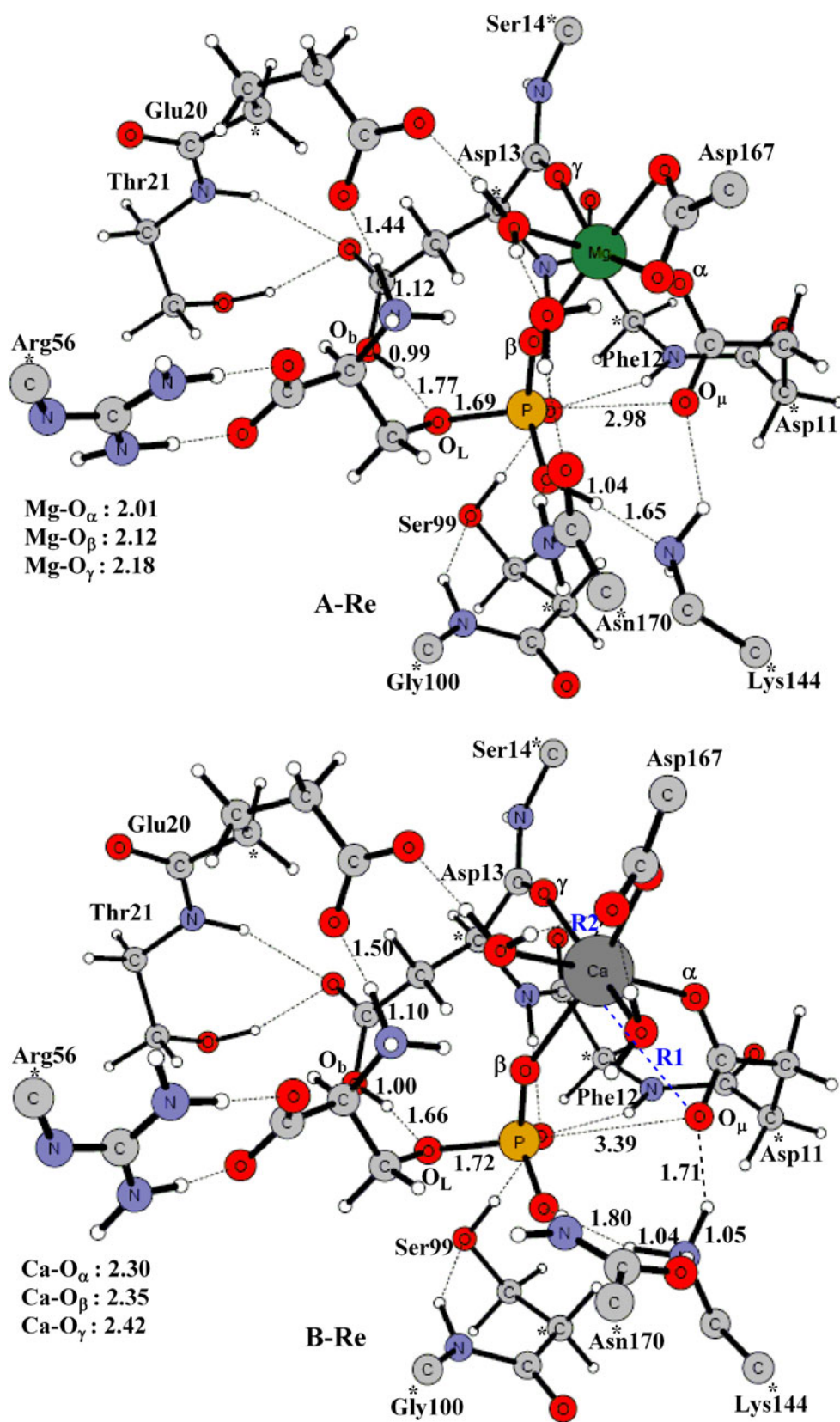
## 4 Results and discussion

### 4.1 Reaction mechanism by PSP with $Mg^{2+}$ ion

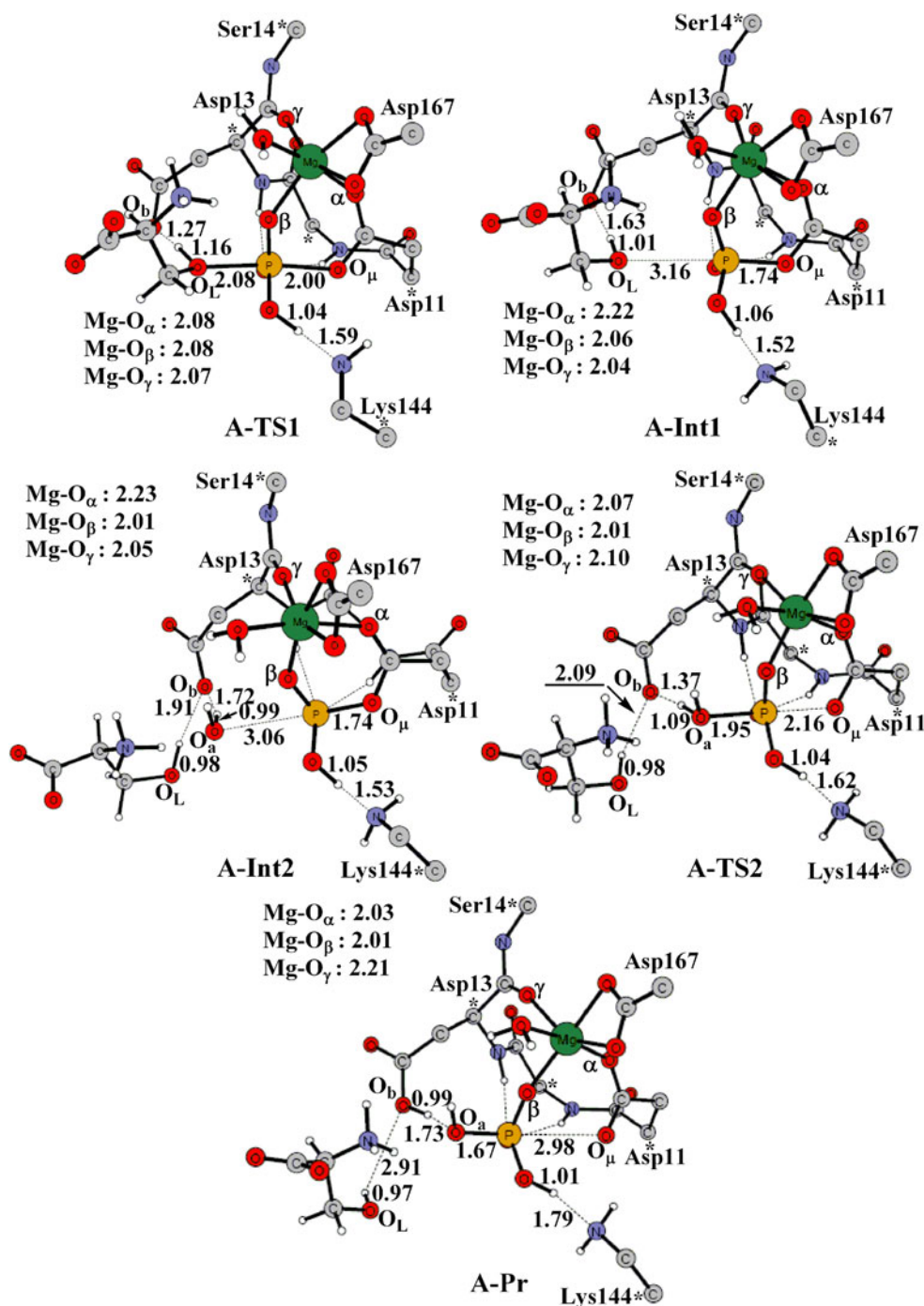
In this study, we first considered the reaction mechanism of PSP with the  $Mg^{2+}$  ion. The optimized structure of the PSP active site model in complex with the PLS substrate (called

**A-Re**) is shown in Fig. 2. Most of geometric parameters obtained from calculations are in good agreement with the experimental structure, except that the  $Mg^{2+}$  ion coordinates to one water molecule and bidentately to Asp167 rather than to two water molecules and monodentately to Asp167 as in the crystal structure, which has also been confirmed by active site model calculations (see Supporting information). The reason could be that the species coordinated to  $Mg^{2+}$  are different, which are a phosphate in the crystal structure and the PLS substrate in **A-Re**. This type of phenomena has also been observed in a number of metalloenzymes and metal model compounds. This type of phenomena, termed as carboxylate shift, has also been observed in other mononuclear metalloenzymes [27, 38, 65–74] and diiron biological systems [75–80] as well as in a number of model complexes [81–90]. This process is proved to be a low-energy process by increasing X-ray structural and DFT evidence [38, 68, 69, 71, 74, 75, 77, 82, 90]. DFT calculations by Dudev and Lim showed that the switch of the binding modes for  $Mg^{2+}$  complexes is associated with rather small energetics [29]. The substrate is coordinated to the magnesium ion with one of its phosphate oxygen atoms and forms several hydrogen bonds to peptide backbone of Asp11-Phe12-Asp13, side chains of Asp13, Glu20, Arg56, Ser99, Lys144, and Asn170. Here, a proton is transferred from Lys144 to the substrate. The energy of the species with the proton at Lys144 is very close to **A-Re**. In addition, transition state optimization shows that this proton must transfer to the phosphate before

**Fig. 2** Optimized structures for the reactant with  $Mg^{2+}$  ion (**A-Re**) and  $Ca^{2+}$  ion (**B-Re**). Atoms marked with *asterisks* were fixed at their X-ray structure positions. For clarity, unimportant hydrogen atoms are not shown. The bond distances are in angstrom



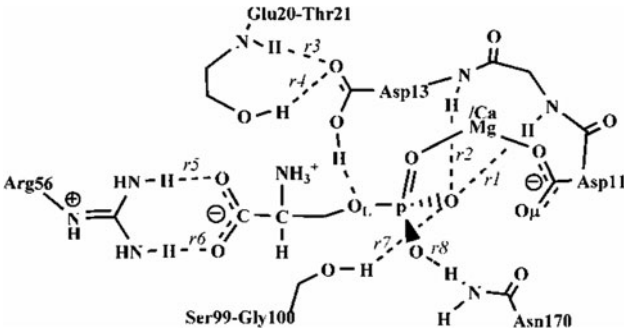
**Fig. 3** Optimized geometries for the transition states, intermediates, and product along the reaction pathway with  $Mg^{2+}$  ion (model A). For clarity, Glu20, Thr21, Arg56, Ser99, Gly100, Asn170, and the uncoordinated water molecule are not shown



reaching the transition state. Therefore, only the case with a neutral Lys144 is presented here. These interactions help orient the substrate and stabilize its negative charge so that there is a nearly straight line between  $O_{\mu}$ , P, and  $O_L$ , with an angle of  $175.2^{\circ}$ . In **A-Re**, the  $P-O_{\mu}$ (Asp11) distance is calculated to be  $2.98 \text{ \AA}$ , which is quite close to the crystallographic distance of  $2.90 \text{ \AA}$  [3].

Starting from **A-Re**, we have optimized the structures of the transition state (**A-TS1**) for the nucleophilic attack by Asp11 and the resulting asparatyl-phosphate intermediate

(**A-Int1**) (see Fig. 3). The barrier is calculated to be  $11.9 \text{ kcal mol}^{-1}$  ( $15.2 \text{ kcal mol}^{-1}$  without solvation correction), and **A-Int1** is found to lie at  $-0.1 \text{ kcal mol}^{-1}$  ( $+3.4 \text{ kcal mol}^{-1}$  without solvation correction) relative to **A-Re**. Our calculations suggest that the nucleophilicity of Asp11 is sufficient enough to perform the attack, which is quite similar to  $\beta$ -phosphoglucomutase ( $\beta$ -PGM) [24] and deoxynucleotidases (dNs) [33], and this step is reversible. This agrees quite well with the fact that L-serine is a negative feedback inhibitor which regulates the metabolic

**Table 1** Important distances (Å) for the various stationary points along the reaction pathways


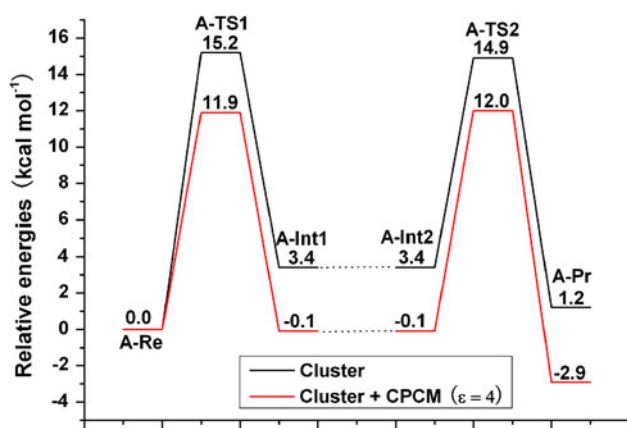
	$r_1$	$r_2$	$r_3$	$r_4$	$r_5$	$r_6$	$r_7$	$r_8$
A-Re	2.14	2.00	2.12	1.92	1.60	1.55	1.82	2.05
A-TS1	2.02	1.88	2.02	1.85	1.64	1.51	1.82	2.07
A-Int1	1.94	2.13	1.99	1.85	1.56	1.49	1.89	2.06
A-Int2	1.91	2.14	1.88	1.86	1.45	1.65	1.86	2.04
A-TS2	2.06	1.87	1.96	1.88	1.50	1.64	1.83	2.01
A-Pr	2.25	1.97	2.01	2.07	1.50	1.66	1.78	2.05
B-Re	2.02	1.92	2.00	1.92	1.60	1.50	1.77	1.74
B-TS1	1.96	1.89	1.92	1.84	1.60	1.46	1.82	1.79
B-Int1	1.89	1.90	1.91	1.84	1.58	1.45	1.81	1.79
B-Int2	1.80	1.97	1.81	1.86	1.41	1.65	1.82	1.72
B-TS2	2.03	1.80	1.86	1.89	1.46	1.66	1.83	1.70
B-Pr	2.06	1.82	1.97	1.95	1.49	1.66	1.72	1.72

activity of PSP [14]. It should be mentioned that QM/MM calculations by Re and coworkers suggested that this step is irreversible [25, 26]. The nature of **A-TS1** is characterized by an imaginary frequency of  $418i \text{ cm}^{-1}$ , which corresponds to the  $\text{P-O}_\mu$  bond formation and  $\text{P-O}_L$  bond cleavage, coupled with proton transfer from Asp13 to  $\text{O}_L$ . Here, Asp13 functions as a general acid to protonate the leaving oxyanion as suggested previously [3, 14, 25, 26]. The use of a neutral carboxylic acid residue to help the departure of the leaving group has also been proposed for several other enzymes, for example, Asp43 in Deoxynucleotidases (dNs) [33], Glu204 in methionine aminopeptidase (MetAP) [49], Asp120 in  $\beta$ -lactamase [51], Glu133 in peptide deformylase [53], Asp356 in the *Yersinia* phosphotyrosine phosphatase [54]. Glu201 in glutamyl cyclase [91], Asp90 in metallo- $\beta$ -lactamase [92], At **A-TS1**, the critical  $\text{P-O}_\mu$  distance is 2.00 Å, and the  $\text{P-O}_L$  bond is elongated to 2.08 Å. Our calculations present an associative character in the phosphoryl transfer mechanism, similarly as proposed by Warshel et al. [93, 94]. However, Re and coworkers results suggested a significant metaphosphate-like character in the transition state [25, 26]. In addition, the transferred proton is 1.27 Å from the Asp13 oxygen and 1.16 Å from  $\text{O}_L$ . The  $\text{Mg-O}_\beta$  bond becomes somewhat shorter (2.08 Å), which indicates that the

magnesium ion provides electrostatic stabilization to the transition state, thereby lowering the barrier.

During the phosphorus transfer, a negative charge is transferred from Asp11 in **A-Re** to Asp13 in **A-Int1**. The second-shell residues, Glu20 and Thr21, donate two hydrogen bonds to Asp13 and provide electrostatic stabilization to the negative charge on Asp13 in **A-Int1**. As seen in Table 1, the hydrogen bond distance between Thr21 and the side chain of Asp13 ( $r_3$ ) decreases from 2.12 Å in **A-Re** to 2.02 Å in **A-TS1**, and further to 1.99 Å in **A-Int1**.

After the release of the L-serine, a water molecule can make the reverse attack on the phosphorus center regenerating the anionic Asp11 [1, 19]. We manually added a water molecule to form a hydrogen bond to the side chain of Asp13, and reoptimized the geometry (called **A-Int2**, Fig. 3). The energy of **A-Int2** is set to be equal to **A-Int1**. In **A-Int2**, the  $\text{P-O}_a$  distance is 3.06 Å. From **A-Int2**, we have optimized the transition state for the water attack (**A-TS2**, Fig. 3). The barrier is calculated to be 12.1 kcal mol<sup>-1</sup> (11.5 kcal mol<sup>-1</sup> without solvation correction) (Fig. 4) relative to **A-Int2**. In **A-TS2**, Asp13 abstracts a proton from the water molecule to generate a hydroxide to perform the attack at the phosphorus center. The geometry of **A-TS2** is found to be quite similar to that of **A-TS1**. The  $\text{P-O}_a$  and  $\text{P-O}_\mu$  distances are 1.95 and 2.16 Å,



**Fig. 4** Potential energy profiles for the dephosphorylation and hydrolysis steps of MJSP with  $Mg^{2+}$  ion

respectively. And the water proton is 1.09 and 1.37 Å from  $O_a$  and  $O_b$ , respectively. This water attack results in the formation of the product complex (**A-Pr**, Fig. 3). The second step is found to be exothermic by 2.8 kcal mol<sup>-1</sup> (2.2 kcal mol<sup>-1</sup> without solvation correction). However, QM/MM calculations show that this step is endothermic by over 20 kcal mol<sup>-1</sup>, implying that the reaction is very hard to take place [26].

The obtained potential energy profile for the phosphoserine hydrolysis reaction is shown in Fig. 4. From this, the calculated energy difference between **A-TS1** and **A-TS2** (around 12 kcal mol<sup>-1</sup>) is too small to be able to unambiguously distinguish which one of them is the rate-limiting step. Experiment rate constant was found to be 20 min<sup>-1</sup> for PSP from *Methanococcus Jannaschii* [1], which can be converted to barriers of about 20.9 kcal mol<sup>-1</sup> using classical transition state theory. The calculated barrier of about 12 kcal mol<sup>-1</sup> is quite feasible but somewhat underestimated compared with the experimental results. However, the QM/MM calculations show a much higher barrier 24.4 kcal mol<sup>-1</sup> [26].

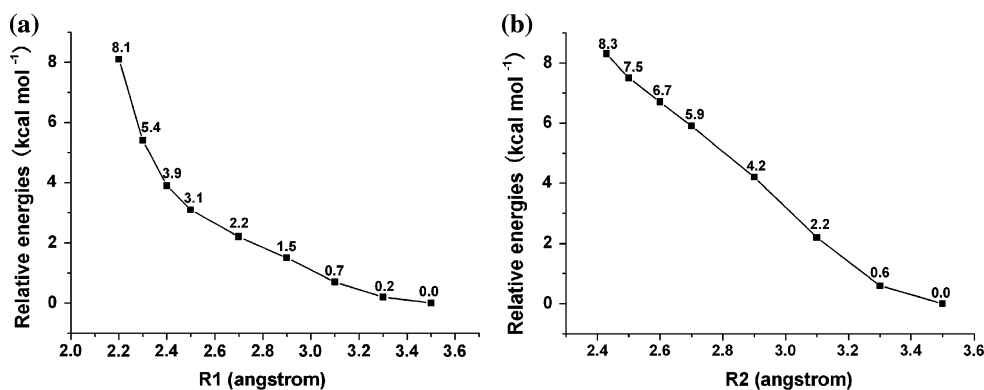
#### 4.2 Inhibition mechanism by PSP with $Ca^{2+}$ ion

To understand the reason for the inhibition by  $Ca^{2+}$  substitution, we use the same active site model as above with  $Ca^{2+}$  as the cofactor to study the hydrolysis reaction of PLS.

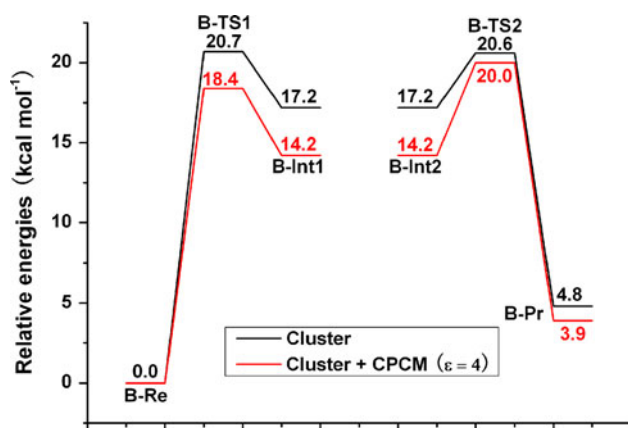
The optimized reactant complex is labeled as **B-Re**, in which the calcium is octahedral coordinated as  $Mg^{2+}$  but with different metal-ligand binding pattern (Seen Fig. 2).  $Ca^{2+}$  coordinates to two water molecules and monodentately to Asp167 and Asp11, and the coordination distances are in the range of 2.3–2.5 Å. This is different from the  $Mg^{2+}$  case, in which the magnesium ion is ligated to one  $H_2O$  and bidentately to Asp167 and the average coordination distance is around 2.1 Å. However, a bidentate coordination mode between  $Ca^{2+}$  and Asp11 was proposed to explain the lack of activity [18, 19, 27, 29]. To confirm that the calcium is hexacoordinated, geometry constrained optimizations have been performed to force the formation of seven-fold coordination between  $Ca^{2+}$  and Asp11, and between  $Ca^{2+}$  and Asp167. As seen from Fig. 5, the decrease in the distances of  $Ca-O_\mu(Asp11)$  and  $Ca-O(Asp167)$  leads to an increase in the energy. For example, when the  $Ca-O_\mu(Asp11)$  bond distance is fixed at 2.3 Å, an energetic penalty of 5.4 kcal mol<sup>-1</sup> is present. Another difference is that Lys144 is preferred to be protonated and there is no need of proton transfer to the phosphate for the reaction. The  $P-O_\mu$  distance is 3.39 Å, which is about 0.4 Å longer than that in **A-Re**. The longer distance implies more energetic requirement for the nucleophilic attack.

The reaction mechanism for the PLS hydrolysis in this case is very similar to that for the  $Mg^{2+}$  case. However, the barrier for the first step is calculated to be 18.4 kcal mol<sup>-1</sup> (20.7 kcal mol<sup>-1</sup> without solvation correction) (see in Fig. 6). This is 6.5 kcal mol<sup>-1</sup> higher than that of **A-TS1**. In addition, the leading intermediate **B-Int1** is found to lie at +14.2 kcal mol<sup>-1</sup> (17.2 kcal mol<sup>-1</sup> without solvation correction) relative to **B-Re**. This indicates that the reverse

**Fig. 5** Computed energy of **B-Re** with R1 (a)/R2 (b) fixed at different distances. The energies are relative to **B-Re**







**Fig. 6** Potential energy profiles for the dephosphorylation and hydrolysis steps of MJPSp with  $\text{Ca}^{2+}$  ion

reaction is much easier to take place than the forward reaction, which is different from the reversible reaction in the  $\text{Mg}^{2+}$  case. In **B-TS1**, the critical  $\text{P-O}_\mu$  distance is 2.25 Å, and the  $\text{P-O}_L$  bond is elongated to 2.34 Å (See Fig. 7). Both are longer than those in the  $\text{Mg}^{2+}$  case. At **B-Int1**, the  $\text{P-O}_\mu\text{-C}_{\text{Asp11}}$  angle is 128.5°, slightly larger than that in **A-Int1** (124.7°), and the  $\text{O}_\beta\text{-Ca-O}_\alpha$  angle is 79.7°, slightly smaller than that in **A-Int1** (84.0°). In addition, the  $\text{P-O}_\mu$  is 1.83 Å, which is 0.09 Å longer than that in **A-Int1**. Thus, the coordination of the phosphoryl-carboxylate intermediate to  $\text{Ca}^{2+}$  induces larger geometric strain and the formation of **B-Int1** requires more energy than that of **A-Int1**.

Similar to the case of  $\text{Mg}^{2+}$ , a water molecule can make a reverse attack on the phosphoryl-carboxylate intermediate, leading to the regeneration of a free Asp11. Calculations show that this step is rate-limiting with a barrier of 20.0 kcal mol<sup>-1</sup> (20.6 kcal mol<sup>-1</sup> without solvation correction), which is about 8 kcal mol<sup>-1</sup> higher than that in the case of  $\text{Mg}^{2+}$ . The optimized transition state (**B-TS2**) and the resulting product complex (**B-Pr**) are shown in Fig. 7. The whole reaction is now endothermic by 3.9 kcal mol<sup>-1</sup>, while it is exothermic by 2.9 kcal mol<sup>-1</sup> in the case of  $\text{Mg}^{2+}$ .

The obtained potential energy profile for the  $\text{Ca}^{2+}$  case is shown in Fig. 6. From this, it can be seen that the second half-reaction determines the hydrolysis kinetics, with an accumulated barrier of 20.0 kcal mol<sup>-1</sup>. Considering a slight underestimation of the barrier for the Mg case, the barrier for the  $\text{Ca}^{2+}$  case should be several kcal mol<sup>-1</sup> higher, which would explain the lack of activity quite well.

As mentioned above, we use the same active site model as  $\text{Mg}^{2+}$  study the inhibition by  $\text{Ca}^{2+}$  substitution. The addition of  $\text{Ca}^{2+}$  with larger ionic radius into the  $\text{Mg}^{2+}$  cavity could introduce strains imposed on active site residues, including Asp167 and Asp11. A number of studies have been done on the consideration of the effect of

constraints in the cluster modeling of enzymatic reactions [95–98]. In general, the effect is quite small, and it usually changes the energy by at most 1–3 kcal mol<sup>-1</sup>, and never alters the mechanistic conclusions. Here, we also performed constrain variations by moving  $\text{C}_\alpha$  atom of Asp11 and Asp167 0.1 and 0.2 Å away from calcium to roughly estimate the effect of constrain and also to check the flexibility of the model. **B-Re** and **B-Int1** were used as two representative stationary points. The distance changes between calcium and  $\text{C}_\alpha$  atom of Asp11 ( $r_{\text{Ca-C1}}$ ) and Asp167 ( $r_{\text{Ca-C49}}$ ) and the energetic changes are rather small. For all cases, the largest deviations of  $r_{\text{Ca-C1}}$  and  $r_{\text{Ca-C49}}$  are 0.5 and 0.2 Å, respectively, compared with the crystal structures. For the 0.2 Å displacements, the two bond distances increase by less than 0.07 Å (see Table S11). Furthermore, the absolute energy increases by at most 2.7 kcal mol<sup>-1</sup>, while the largest deviation of relative energy is 2.2 kcal mol<sup>-1</sup> (see Table S12). Thus, the effect is quite small and the use of the present active site model designed on the basis of the crystal structure is able to capture the factors that control the metal selectivity of this enzyme.

## 5 Conclusions

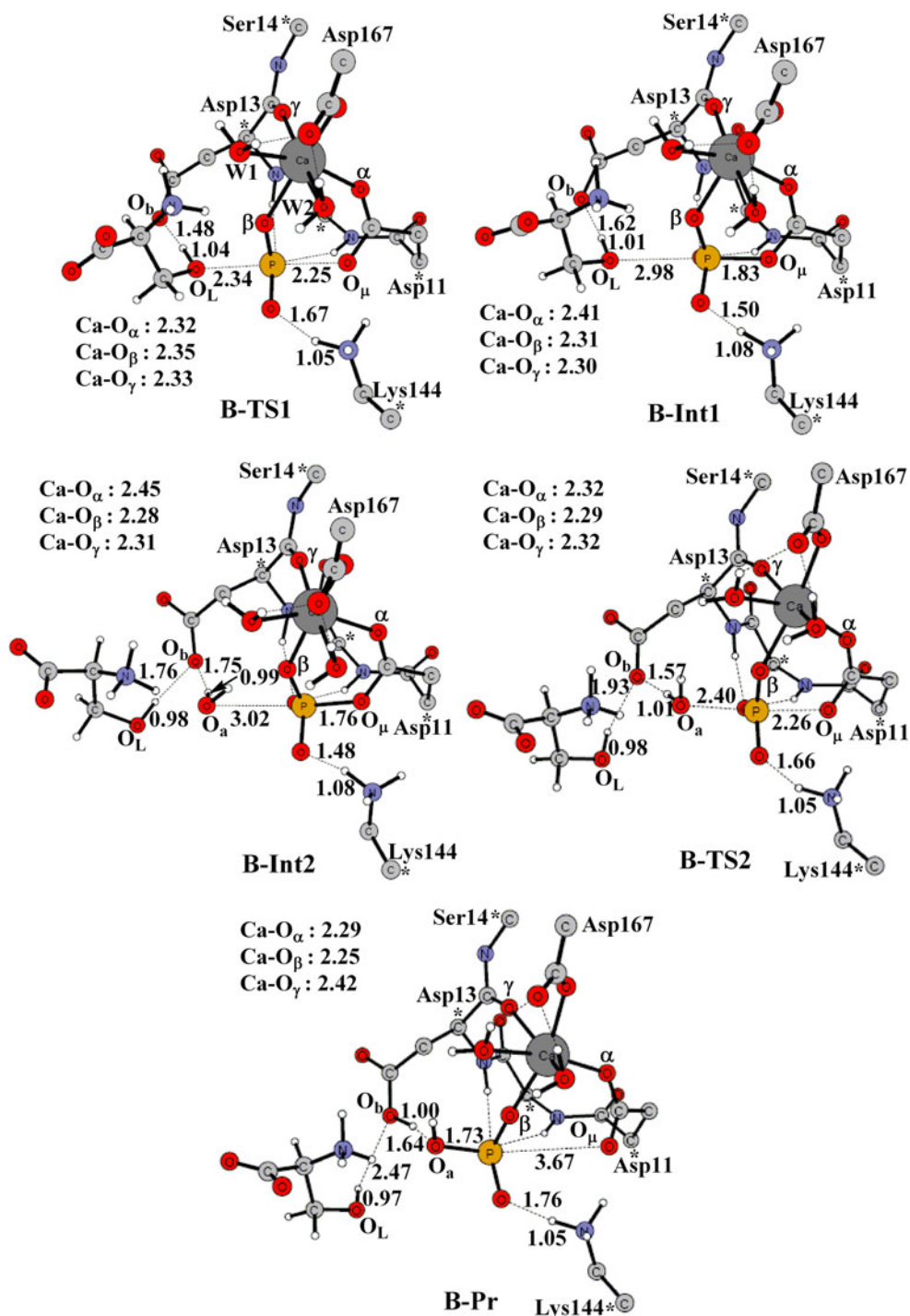
In the present paper, we have used a large quantum cluster model to investigate the reaction mechanism of  $\text{Mg}^{2+}$ -dependent PSP and the lack of activity by  $\text{Ca}^{2+}$  substitution. Our calculations give support to previous mechanistic suggestions based on QM/MM calculations (Scheme 2) [25, 26] but give more reasonable potential energy profile. The hydrolysis proceeds through two steps. In the first step, Asp11 performs the nucleophilic attack on the phosphorus moiety, concertedly with the departure of the leaving group, facilitated by proton transfer from Asp13 to the alkoxide. In the subsequent step, Asp13 activates a water molecule to make a reverse attack, regenerating an anionic Asp11. The calculated barriers for both steps are ca 12 kcal mol<sup>-1</sup>, which is in good agreement with the experimental kinetics.

The substitution of  $\text{Mg}^{2+}$  by  $\text{Ca}^{2+}$  results in ca 8 kcal mol<sup>-1</sup> higher barrier for the hydrolysis. The formation of the phosphoryl-carboxylate intermediate is endothermic by as much as 14 kcal mol<sup>-1</sup>. The main reason is that the  $\text{Ca}^{2+}$  introduces larger geometric strain on the intermediate.

## 6 Supporting information available

Optimized structure for the active site of MJPSp in complex with a phosphate group bound. Important distances (Å) and energies for constrain variations by moving  $\text{C}_\alpha$

**Fig. 7** Optimized geometries for the transition states, intermediates, and product along the reaction pathway with  $\text{Ca}^{2+}$  ion (model B). For clarity, Glu20, Thr21, Arg56, Ser99, Gly100, and Asn170 are not shown



atom of Asp11 and Asp167 0.1 and 0.2 Å away from calcium using **B-Re** and **B-Int1** as two representative stationary points, respectively.

**Acknowledgments** We appreciate Dr. Sven de Marothy (from Stockholm University) for providing xyzviewer to create all the figures. This work was supported by grants from the National Natural Science Foundation of China (grant nos. 20733002, 20873008, 21073014, and 21203042), the Fundamental Research Funds for the Central Universities (Grant No. HIT. NSRIF. 2013057), and Major

State Basic Research Development Programs (grant nos. 2004CB719903 and 2002CB613406).

## References

1. Wang W, Cho Ho S, Kim R, Jancarik J, Yokota H, Nguyen HH, Grigoriev Igor V, Wemmer DE, Kim S-H (2002) J Mol Biol 319:421–431

2. Kim H-Y, Heo Y-S, Kim JH, Park MH, Moon J, Kim E, Kwon D, Yoon J, Shin D, Jeong E, Park SY, Lee TG, Jeon YH, Ro S, Cho JM, Hwang KY (2002) *J Biol Chem* 277:46651–46658
3. Wang W, Kim R, Jancarik J, Yokota H, Kim S-H (2001) *Structure* 9:65–71
4. Wolosker H, Sheth KN, Takahashi M, Mothet J-P, Brady RO Jr, Ferris CD, Snyder SO (1999) *Proc Natl Acad Sci USA* 96:721–725
5. Dunlop DS, Neidle A (1997) *Biochem Biophys Res Commun* 235:26–30
6. Matsui T, Sekiguchi M, Hashimoto A, Tomita U, Nishikawa T, Wada K (1995) *J Neurochem* 65:454–458
7. Berger AJ, Dieudonné S, Ascher P (1998) *J Neurophysiol* 80:3336–3340
8. Sugiura N, Patel RG, Corriveau RA (2001) *J Biol Chem* 276:14257–14263
9. Wood PL (1995) *Life Sci* 57:301–310
10. Paudice P, Gemignani A, Raiteri M (1998) *Eur J Neurosci* 10:2934–2944
11. Veeranna, Shetty KT (1991) *Neurochem Res* 15:1203–1210
12. Hawkinson JE, Acosta-Burrueal M, Ta ND, Wood PL (1997) *Eur J Pharmacol* 337:315–324
13. Collet J-F, Stroobant V, Van Schaftingen E (1999) *J Biol Chem* 274:33985–33990
14. Collet J-F, Stroobant V, Pirard M, Delpierre G, Van Schaftingen E (1998) *J Biol Chem* 273:14107–14112
15. MacLennan DH, Clarke DM, Loo TW, Skerjanc IS (1992) *Acta Physiol Scand Suppl* 607:141–150
16. Lingrel JB, Kuntzweiler T (1994) *J Biol Chem* 269:19659–19662
17. Cho H, Wang W, Kim R, Yokota H, Damo S, Kim S-H, Wemmer D, Kustu S, Yan D (2001) *Proc Natl Acad Sci USA* 98:8525–8530
18. Peeraer Y, Rabijns A, Collet J-F, Van Schaftingen E, De Ranter C (2004) *Eur J Biochem* 271:3421–3427
19. Peeraer Y, Rabijns A, Verboven C, Collet J-F, Van Schaftingen E, De Ranter C (2003) *Acta Cryst D59*:971–977
20. Rinaldo-Matthis A, Rampazzo C, Reichard P, Bianchi V, Nordlund P (2002) *Nat Struct Biol* 9:779–787
21. Hisano T, Hata Y, Fujii T, Liu JQ, Kurihara T, Esaki N, Soda K (1996) *J Biol Chem* 271:20322–20330
22. Toyoshima C, Nakasako M, Nomura H, Ogawa H (2000) *Nature* 405:647–655
23. Lahiri SD, Zhang GF, Dunaway-Mariano D, Allen KN (2003) *Science* 299:2067–2071
24. Allegrini S, Scaloni A, Ferrara L, Pesi R, Pinna P, Sgarrella F, Camici M, Eriksson S, Tozzi MG (2001) *J Biol Chem* 276:33526–33532
25. Re S, Jung J, Ten-no S, Sugita Y (2009) *Chem Phys Lett* 480:284–288
26. Re S, Imai T, Jung J, Ten-no S, Sugita Y (2011) *J Comput Chem* 32:260–270
27. Dudev T, Lim C (2007) *Acc Chem Res* 40:85–93
28. Babu CS, Dudev T, Casareno R, Cowan JA, Lim C (2003) *J Am Chem Soc* 125:9318–9328
29. Dudev T, Lim C (2004) *J Phys Chem B* 108:4546–4557
30. Becke AD (1993) *J Chem Phys* 98:1372–1377
31. Becke AD (1993) *J Chem Phys* 98:5648–5652
32. Lee C, Yang W, Parr RG (1988) *Phys Rev B* 37:785–789
33. Himo F, Guo J-D, Rinaldo-Matthis A, Nordlund P (2005) *J Phys Chem B* 109:20004–20008
34. Himo F, Siegbahn PEM (2003) *Chem Rev* 103:2421–2456
35. Noodleman L, Lovell T, Han W-G, Li J, Himo F (2004) *Chem Rev* 104:459–508
36. Siegbahn PEM, Borowski T (2006) *Acc Chem Res* 39:729–738
37. Himo F (2006) *Theo Chem Acc* 116:232–240
38. Ramos MJ, Fernandes PA (2008) *Acc Chem Res* 41:689–698
39. Chen S-L, Fang W-H, Himo F (2007) *J Phys Chem B* 111:1253–1255
40. Liao R-Z, Yu J-G, Himo F (2011) *J Inorg Biochem* 105:927–936
41. Liao R-Z, Yu J-G, Raushel FM, Himo F (2008) *Chem Eur J* 14:4287–4292
42. Liao R-Z, Yu J-G, Himo F (2009) *Inorg Chem* 48:1442–1448
43. Chen S-L, Fang W-H, Himo F (2009) *J Inorg Biochem* 103:274–281
44. Yang L, Liao R-Z, Yu J-G, Liu R-Z (2009) *J Phys Chem B* 113:6505–6510
45. Liao R-Z, Himo F, Yu J-G, Liu R-Z (2009) *Eur J Inorg Chem* 20:2967–2972
46. Liao R-Z, Himo F, Yu J-G, Liu R-Z (2010) *J Inorg Biochem* 104:37–46
47. Yang L, Liao R-Z, Himo F, Yu J-G (2010) *J Phys Chem B* 114:2533–2540
48. Liao R-Z, Himo F, Yu J-G (2010) *Inorg Chem* 49:6883–6888
49. Leopoldini M, Russo N, Toscano M (2007) *J Am Chem Soc* 129:7776–7784
50. Abashkin YG, Burt SK, Collins JR, Cachau RE, Russo N, Erickson JW (1996) In: Russo N, Salahub DR (eds) *Metal-ligand interactions: structure and reactivity*, Nato Science Series. Kluwer, Dordrecht
51. Olsen L, Anthony J, Ryde U, Adolph H-W, Hemmingsen L (2003) *J Phys Chem B* 107:2366–2375
52. Marino T, Russo N, Toscano M (2005) *J Am Chem Soc* 127:4242–4253
53. Leopoldini M, Russo N, Toscano M (2006) *J Phys Chem B* 110:1063–1072
54. Zhang ZY (1998) *Crit Rev Biochem Mol Biol* 33:1–52
55. Frisch MJ, Trucks GW, Schlegel HB, Scuseria GE, Robb MA, Cheeseman JR, Montgomery JA Jr, Vreven T, Kudin KN, Burant JC, Millam JM, Iyengar SS, Tomasi J, Barone V, Mennucci B, Cossi M, Scalmani G, Rega N, Petersson GA, Nakatsuji H, Hada M, Ehara M, Toyota K, Fukuda R, Hasegawa J, Ishida M, Nakajima T, Honda Y, Kitao O, Nakai H, Klene M, Li X, Knox JE, Hratchian HP, Cross JB, Adamo C, Jaramillo J, Gomperts R, Stratmann RE, Yazyev O, Austin AJ, Cammi R, Pomelli C, Ochterski JW, Ayala PY, Morokuma K, Voth GA, Salvador P, Dannenberg JJ, Zakrzewski VG, Dapprich S, Daniels AD, Strain MC, Farkas O, Malick DK, Rabuck AD, Raghavachari K, Foresman JB, Ortiz JV, Cui Q, Baboul AG, Clifford S, Cioslowski J, Stefanov BB, Liu G, Liashenko A, Piskorz P, Komaromi I, Martin RL, Fox DJ, Keith T, Al-Laham MA, Peng CY, Nanayakkara A, Challacombe M, Gill PMW, Johnson B, Chen W, Wong MW, Gonzalez C, Pople JA (2004) *Gaussian 03*, revision C02. Gaussian, Inc., Wallingford
56. Zhao Y, Truhlar DG (2004) *J Phys Chem A* 108:6908–6918
57. Zhao Y, Truhlar DG (2008) *Acc Chem Res* 41:157–167
58. Barone V, Cossi M (1998) *J Phys Chem A* 102:1995–2001
59. Cammi R, Mennucci B, Tomasi J (1999) *J Phys Chem A* 103:9100–9108
60. Klamt A, Schüürmann G (1993) *J Chem Soc Perkin Trans 2*:799–805
61. Tomasi J, Mennucci B, Cammi R (2005) *Chem Rev* 105:2999–3093
62. Hu P, Zhang Y (2006) *J Am Chem Soc* 128:1272–1278
63. Senn HM, Thiel S, Thiel W (2005) *J Chem Theory Comput* 1:494–505
64. Senn HM, Kästner J, Breidung J, Thiel W (2009) *Can J Chem* 87:1322–1337
65. Sousa SF, Fernandes PA, Ramos MJ (2009) *Chem Eur J* 15:4243–4247
66. Sousa SF, Fernandes PA, Ramos MJ (2007) *J Am Chem Soc* 129:1378–1385
67. Sousa SF, Fernandes PA, Ramos MJ (2005) *J Mol Struct: THEOCHEM* 729:125–129

68. Sousa SF, Fernandes PA, Ramos MJ (2005) *J Biol Inorg Chem* 10:3–10
69. Sousa SF, Fernandes PA, Ramos MJ (2005) *Biophys J* 88:483–494
70. Sousa SF, Fernandes PA, Ramos MJ (2007) *J Comput Chem* 28:1160–1168
71. Ryde U (1999) *Biophys J* 77:2777–2787
72. Tamames B, Sousa SF, Tamames J, Fernandes PA, Ramos MJ (2007) *Proteins: Struct, Funct, Bioinf* 69:466–475
73. Robert V, Lemerrier G (2006) *J Am Chem Soc* 128:1183–1187
74. Szeto MWY, Mujika JI, Zurek J, Mulholland AJ, Harvey JN (2009) *J Mol Struct: THEOCHEM* 898:106–114
75. Torrent M, Musaev DG, Morokuma K (2001) *J Phys Chem B* 105:322–327
76. Gherman BF, Baik MH, Lippard SJ, Friesner RA (2004) *J Am Chem Soc* 126:2978–2990
77. Voegtli WC, Khidekel N, Baldwin J, Ley BA, Bollinger JM, Rosenzweig AC (2000) *J Am Chem Soc* 122:3255–3261
78. Rosenzweig AC, Nordlund P, Takahara PM, Frederick CA, Lippard SJ (1995) *Chem Biol* 2:409–418
79. Whittington DA, Lippard S (2001) *J Am Chem Soc* 123:827–838
80. Dunietz BD, Beachy MD, Cao YX, Whittington DA, Lippard SJ, Friesner RA (2000) *J Am Chem Soc* 122:2828–2839
81. Paterová J, Heyda J, Jungwirth P, Shaffer CJ, Révész Á, Zins EL, Schröder D (2011) *J Phys Chem A* 115:6813–6819
82. Demsar A, Kosmrlj J, Petricek S (2002) *J Am Chem Soc* 124:3951–3958
83. Lemerrier G, Mulliez E, Brouca-Cabarrecq C, Dahan F, Tuchaques JP (2004) *Inorg Chem* 43:2105–2113
84. Kuzelka J, Spingler B, Lippard SJ (2002) *Inorg Chim Acta* 337:212–222
85. Rardin RL, Bino A, Poganiuch P, Tolman WB, Liu S, Lippard SJ (1990) *Angew Chem Int Ed* 29:812–814
86. Baffert C, Collomb MN, Deronzier A, Kjaergaard-Knudsen S, Latour JM, Lund KH, McKenzie CJ, Mortensen M, Nielsen L, Thorup N (2003) *J Chem Soc, Dalton Trans* 9:1765–1772
87. Pursche D, Triller MU, Reddig N, Rompel A, Krebs BZ (2003) *Anorg Allg Chem* 629:24–28
88. Feig AL, Masschelein A, Bakac A, Lippard SJ (1997) *J Am Chem Soc* 119:334–342
89. Ducháčková L, Schröder D, Roithová J (2011) *Inorg Chem* 50:3153–3158
90. LeCloux DD, Barrios AM, Mizoguchi TJ, Lippard SJ (1998) *J Am Chem Soc* 120:9001–9014
91. Calvaresi M, Garavelli M, Bottoni A (2008) *Proteins* 73:527–538
92. Bounaga S, Laws AP, Galleni M, Page MI (1998) *Biochem J* 331:703–711
93. Åqvist J, Kolmodin K, Florian J, Warshel A (1999) *Chem Biol* 6:R71–R80
94. Klähn M, Rosta E, Warshel A (2006) *J Am Chem Soc* 128:15310–15323
95. Pelmeshikov V, Blomberg MRA, Siegbahn PEM (2002) *J Biol Inorg Chem* 7:284–298
96. Pelmeshikov V, Siegbahn PEM (2002) *Inorg Chem* 41:5659–5666
97. Siegbahn PEM (2004) *J Biol Inorg Chem* 9:577–590
98. Siegbahn PEM (2011) *ChemPhysChem* 12:3274–3280